Self-limited hyperexcitability: functional effect of a familial hemiplegic migraine mutation of the Nav1.1 (SCN1A) Na+ channel.

Sandrine Cestèle, Paolo Scalmani, Raffaella Rusconi, Benedetta Terragni, Silvana Franceschetti, Massimo Mantegazza

Self-limited hyperexcitability: functional effect of a familial hemiplegic migraine mutation of the $Na_v1.1$ (SCN1A) Na+ channel

Cestèle Sandrine [1 2], Scalmani Paolo [1], Rusconi Raffaella [1], Terragni Benedetta [1], Franceschetti Silvana [1], Mantegazza Massimo [1 *]

[1] *Department of Neurophysiopathology Besta Neurological Institute, 20133 Milan,IT*

[2] *GIN, Grenoble Institut des Neurosciences INSERM : U836, CEA, Université Joseph Fourier - Grenoble I, CHU Grenoble, UJF - Site Santé La Tronche BP 170 38042 Grenoble Cedex 9,FR*

* Correspondence should be adressed to: Massimo Mantegazza <mmantegazza@istituto-besta.it>

Abstract

Familial hemiplegic migraine (FHM) is an autosomal dominant inherited subtype of severe migraine with aura. Mutations causing FHM (type 3) have been identified in SCN1A, the gene encoding neuronal voltage gated $Na_v1.1$ Na^+ channel α subunit, but functional studies have been done using the cardiac $Na_v1.5$ isoform and the observed effect were similar to those of some epileptogenic mutation. We studied the FHM mutation Q1489K transfecting tsA-201 cells and cultured neurons with human $Na_v1.1$. We show that the mutation has effects on the gating properties of the channel that can be consistent with both hyperexcitability and hypoexcitability. Simulation of neuronal firing and long depolarizing pulses mimicking pro-migraine conditions revealed that the effect of the mutation is a gain of function consistent with increased neuronal firing. However, during high frequency discharges and long depolarizations the effect becomes a loss of function. This potent but self-limited capacity to induce neuronal hyperexcitability may be a specific characteristic of migraine mutations, able to both trigger the cascade of events that leads to migraine and counteract the development of extreme hyperexcitability typical of epileptic seizures. Thus, we disclosed at the channel biophysical level a possible difference in the pathogenic mechanism of two major diseases.

MESH Keywords Action Potentials ; genetics ; physiology ; Animals ; Cell Line ; Cells, Cultured ; Glutamine ; genetics ; Humans ; Ion Channel Gating ; genetics ; physiology ; Lysine ; genetics ; Migraine with Aura ; genetics ; metabolism ; physiopathology ; Mutation ; Nerve Tissue Proteins ; genetics ; physiology ; Patch-Clamp Techniques ; Protein Subunits ; genetics ; physiology ; Rats ; Sodium Channels ; genetics ; physiology

Introduction

Migraine is a common disease with a strong genetic component. About 35% of migraine patients have migraine with aura, consisting of transient focal neurological symptoms (often visual disturbances) that precede the headache (Pietrobon and Striessnig, 2003;Kors et al., 2004;Silberstein, 2004).

Functional studies in patients have provided evidence that the visual aura coincides with cortical spreading depression (CSD) (Bowyer et al., 2001;Hadjikhani et al., 2001), a wave of neuronal depolarization that spreads slowly across the cerebral cortex and generates a transient intense firing activity followed by a long lasting suppression (Pietrobon and Striessnig, 2003). The headache is caused by the stimulation of trigeminal fibers that innervate the blood vessels of the meninges and activate brain areas involved in the perception of pain (Pietrobon and Striessnig, 2003). Experiments in animal models have shown that CSD can activate this pain pathway (Bolay et al., 2002), but it is not clear what is the trigger of CSD and what is the mechanism that links CSD to activation of nociceptors.

Causative genes have been identified for familial hemiplegic migraine (FHM), a severe autosomal dominant inherited subtype of migraine with aura characterized by hemiparesis during the attacks (Pietrobon and Striessnig, 2003;Kors et al., 2004;Pietrobon, 2007). FHM type 1 is caused by gain-of-function mutations of the α1-subunit of neuronal $Ca_v1.2$ Ca^{2+} channel (Ophoff et al., 1996), consistently with enhanced glutamate release (Pietrobon, 2007); facilitation of CSD was observed in a knock-in mouse model (van den Maagdenberg et al., 2004). FHM type 2 is caused by loss of function mutations of the α2 subunit of the Na^+/K^+ pump (ATP1A2) (De Fusco et al., 2003), consistently with reduced removal of K^+ and glutamate from the extracellular space, thus with inhibition of recovery from neuronal excitation, long lasting depolarizations and CSD (Pietrobon, 2007).

More recently, FHM (type 3) mutations have been identified in SCN1A, the gene encoding neuronal voltage gated $Na_v1.1$ Na^+ channel α subunit (Dichgans et al., 2005;Vanmolkot et al., 2007). Because of difficulties in handling $Na_v1.1$ cDNA, the functional study of FHM3 mutations has been done using the cardiac $Na_v1.5$ Na^+ channel. However, $Na_v1.1$ is the major target of epileptogenic mutations and some of them have functional effects that are similar to those reported for migraine mutations studied with $Na_v1.5$ (Meisler and Kearney, 2005;Avanzini et al., 2007), complicating our understanding of the differential pathogenetic mechanism of the two diseases. Thus, it is important to study the functional effects of migraine mutations in the human $Na_v1.1$ clone. In fact, despite their high level of homology, cardiac and neuronal Na^+ channels show several structural and functional differences (Kirsch and Brown, 1989;Richmond et al., 1998; Mantegazza et al., 2001;Catterall et al., 2005;Mantegazza et al., 2005b).

We introduced the FHM mutation Q1489K into $hNa_v1.1$ Na^+ channel cDNA (Q1478K according to the numeration of the $hNa_v1.1$ clone that we have used, see results), and we studied its functional effects in transfected human tsA-201 cell line and rat cultured neurons, shedding light on the possible pathogenic mechanism that differentiates $Na_v1.1$ migraine mutations from epileptogenic mutations.

Methods

Site-directed mutagenesis

The human clone of the shorter splice variant isoform (1998 amino acids) of $Na_v1.1$ Na^+ channel (Schaller et al., 1992) was donated by Dr. Jeff.Clare (GlaxoSmithKline, Stevenage, Herts, UK). We subcloned it into the plasmid pCDM8 (Mantegazza et al., 2005a), which was propagated in Top 10/P3 bacteria (Invitrogen), grown at 30°C for about 48 hours in order to minimize rearrangements. The mutation Q1478K was introduced into pCDM8-$hNa_v1.1$ by means of the Quick Change XL site directed mutagenesis kit (Stratagene) with the following primers: 5′TTCAACCAGAAGAAAAAGAAGTTTGG (forward) and 5′TCTTTTTCTTCTGGTTGAAATTATC (reverse). Colonies were screened by sequencing. We sequenced the whole open reading frame of hNav1.1 after each propagation in order to exclude the presence of spurious mutations.

Transient expression

TsA-201 cells were maintained and transfected with $CaPO_4$ as in (Mantegazza and Cestele, 2005). We cotransfected pCDM8-$hNa_v1.1$ and hβ1 using a 1:2 molar ratio. hβ1 was in the bicistronic plasmid pIRES-YFP (Clontech), which expresses both the protein of interest and yellow fluorescent protein (YFP) as reporter. We did control experiments without β1 (cotransfecting empty pEYFP-N1 as reporter) obtaining similar results (not shown). Neurons were prepared, cultured and transfected as in (Scalmani et al., 2006). Briefly, neocortical neurons were isolated from P1-P3 CD rat pups (Charles River, Civate, Italy). Rats were decapitated under ether anesthesia, the brain was quickly removed, the cerebral cortex was isolated using fine tweezers and chopped into small pieces that were digested with protease type XIV 1 mg/ml (Sigma, St.Louis, MO) for 15min. The tissue was then mechanically dissociated using a series of fire-polished Pasteur pipettes. The dissociated neurons were plated in Petri dishes and cultured at 37°C and with 5%CO_2 in Neurobasal A culture medium (Invitrogen, Carlsbad, CA) supplemented with B27 (Invitrogen), glutamine 1mM (Invitrogen), β-FGF 10ng/ml (Invitrogen), penicillin G 50U/ml and streptomycin 50μg/ml (Sigma). The neurons were transfected on the same day with Lipofectamine 2000 (Invitrogen) and used within 30h..

Electrophysiological recordings and analysis

Transfected cells were selected visually by their fluorescence and recordings were done at room temperature (22–25°C) using a Multiclamp 700A patch-clamp amplifier and pClamp 8.2 software (Molecular Devices). Signals were filtered at 10 KHz and sampled at 100kHz.

We recorded Na^+ currents from tsA-201 cells with the whole-cell configuration of the patch-clamp technique. Recordings were usually started 5 min after the rupture of the membrane patch, in order to allow intracellular dialysis with the pipette solution. External bath solution contained (mM): 150 NaCl, 10 Cs-Hepes, 1 $MgCl_2$, 2 KCl, 1.5 $CaCl_2$, pH 7.4; internal pipette solution was (mM): 105 CsF, 35 NaCl, 10 Cs-Hepes, 10 EGTA, pH 7.4. Cell capacitance and series resistance errors were carefully compensated (~85%) throughout the experiment. Pipette resistance was between 1.5 and 2.0 MΩ and series resistance was between 2.5 and 4.5MΩ; maximum accepted voltage clamp error was 2.5mV. The remaining linear capacity and leakage currents were eliminated online using a P/4 subtraction paradigm.

Macroscopic Na^+ currents were recorded from cultured neurons using the on-cell macropatch configuration of the patch-clamp technique in order to avoid the space clamp errors caused by the long cellular processes (Scalmani et al., 2006). We used different recording solutions than with tsA-201 cells, in order to selectively record Na^+ currents, blocking the endogenous contaminating currents that are present in neurons. The internal pipette solution contained (in mM): 110 NaCl, 35 tetraethylammonium-Cl, 1 $CaCl_2$, 2 $MgCl_2$, 0.3 $NiCl_2$, 0.4 $CdCl_2$, 1.5 4-aminopyridine and 10 Na-HEPES, pH 7.4. The bath solution contained (in mM): 40 K-gluconate, 100 KCl, 5 EGTA, 10 K-HEPES, and 30 glucose, pH 7.4. Capacitative currents were minimized by means of the amplifier circuitry. Series resistance compensation was not used because the maximum peak amplitude of Na^+ currents was less than 270pA. The remaining transient and leakage currents were eliminated using P/4 subtraction. The diameter of the tip (about 3μm) and the shape of the pipettes were kept constant in order to maintain the area of the membrane patch approximately constant. Pipette resistance was between 2.6 and 3.0 MΩ.

All the recordings were corrected for junction potential errors using the pClamp calculation system (Barry, 1994). Conductance-voltage curves were derived from current-voltage (I-V) curves according to $G = I/(V-V_R)$ where I is the peak current, V is the test voltage and V_R is the apparent reversal potential. The voltage dependence of activation and voltage dependence of inactivation were fitted to Boltzmann relationship of the form $1/(1+\exp((V_{1/2}-V)/k))$ plus a baseline, where $V_{1/2}$ is the voltage of half maximal activation (Va) or inactivation (Vh) and k is a slope factor (in mV). Action potentials were recorded from layer V pyramidal neurons in rat

neocortical slices as previously described (Mantegazza et al., 1998), sampled at 30 kHz and used as voltage stimuli in voltage-clamp experiments (Scalmani et al., 2006). Fits were achieved using the Levenberg–Marquardt algorithm with Origin 7.5 (OriginLab, Northampton, MA). The fitting lines in the figures were obtained using mean parameters calculated averaging the parameters of the fits of the single cells. Statistical analyses were made using Origin. The results are given as mean±SEM, and statistical significance was at $p = 0.05$. Statistical comparisons were performed with the t test.

Results

In our study we used the human clone of the shorter splice variant isoform of $Na_v1.1$ Na^+ channel α subunit (Noda et al., 1986;Schaller et al., 1992), which has a deletion of 11 amino acids and could be the predominant $Na_v1.1$ variant expressed in brain (Schaller et al., 1992). The clone has already been used for functional studies (Oliveira et al., 2004;Mantegazza et al., 2005a;Mantegazza et al., 2005b;Rusconi et al., 2007). We introduced in $hNa_v1.1$ the Q1489K FHM3 mutation (Dichgans et al., 2005), which we denominated Q1478K according to the numeration of the clone that we used, and investigated its functional effects by patch-clamp recordings in transiently transfected tsA-201 cells and neocortical cultured neurons.

Voltage-gated Na^+ channel α subunits are formed by four homologous domains (DI-DIV), each containing six transmembrane segments (S1–S6) connected by extra- and intracellular loops; the S4 of each domain constitute the voltage sensor. The mutation Q1478K is located in the cytoplasmic loop between DIII and DIV, the inactivation gate that plugs the pore during fast inactivation (Catterall, 2000).

Effect of Q1478K on the functional properties of $hNa_v1.1$ in tsA-201 cells

Activation and persistent current

Fig. 1A shows representative whole-cell Na^+ current traces recorded over a range of potentials in tsA-201 cells transfected with wild type $hNa_v1.1$ or the migraine mutant $hNa_v1.1$-Q1478K. The time course of activation was not modified by the mutation, as shown by the comparison on a shorter time scale of the mean current traces elicited by depolarizing steps to −5mV displayed in Fig. 1B. The current decay of both $hNa_v1.1$ and $hNa_v1.1$-Q1478K showed a large rapidly inactivating component (I_{NaT}), reflecting inactivation from the open state of the channel, followed by a slowly inactivating “persistent” component (I_{NaP}) that failed to inactivate by the end of long depolarizing steps of up to 150ms (Fig. 1B, inset). The faster component of the decay was not modified by the mutation, but I_{NaP} was consistently larger for $hNa_v1.1$-Q1478K (see below).

The mean current density-voltage plots of I_{NaT} obtained applying test pulses to membrane potentials between −60mV and +80mV are shown in Fig. 1C. I_{NaT} began to activate at about −50mV, peaked at −15 mV and inverted at about +40mV both with wild type and $hNa_v1.1$-Q1478K, but the mutant showed a significant 29% reduction in maximum current density, which is consistent with reduced excitability in neurons expressing the mutant channel. Consistently with the results obtained with the current density-voltage plots, the analysis of the conductance-voltage plots (Fig. 1D) did not show any significant modifications of the activation curve of I_{NaT}.

We quantified I_{NaP} by measuring the average current between 40 and 50 ms after the beginning of the test pulse. Fig. 1E shows the comparison over a range of potentials of the mean I_{NaP} recorded 5min after the establishment of the whole-cell configuration, expressed as percentage of maximum I_{NaT}. I_{NaP} began to activate at about −55mV, peaked at −20mV and inverted at about +40mV, both with wild-type and $hNa_v1.1$- Q1478K. I_{NaP} in cells transfected with $hNa_v1.1$-Q1478K was 3.9-fold larger at −20mV than with the wild type and significantly larger in the whole range of potentials (Fig 1E), a modification that is consistent with increased neuronal excitability. The increase of I_{NaP} induced by the mutation was statistically significant also considering the reduction of the amplitude of I_{NaT} that we observed with $hNa_v1.1$-Q1478K (2.9- fold larger at −20mV). However, comparing I_{NaP} after more than 17min from the establishment of the whole-cell configuration, the increase induced by the mutation was no longer observable (Fig 1F). Thus, the increase of I_{NaP} is a labile property of the mutant that is inhibited by a long-lasting dialysis of the cytoplasm.

Fast Inactivation

We studied the voltage dependence of fast inactivation (Fig. 2A) applying 100ms-long inactivating prepulses to potentials from −110mV to −5mV, followed by a test pulse to −5mV. The inactivation curve of $hNa_v1.1$-Q1478K showed a significant positive shift of 4.1mV and, consistently with the increase of I_{NaP}, its baseline was larger than for the wild-type. Nevertheless, the positive shift of the voltage dependence of inactivation caused by Q1478K may be due to a slower development of fast inactivation of $hNa_v1.1$-Q1478K, which could make the 100ms inactivating prepulse that we used not sufficiently long to induce steady-state fast inactivation. Therefore, we studied the kinetics of development of fast inactivation applying inactivating prepulses of increasing duration to potentials between −75 and −45mV. The curves of both wild type and $hNa_v1.1$-Q1478K were well fit by a single exponential relationship, as shown by the mean curves obtained with depolarizing pulses to −65mV, displayed in Fig. 2B. However, the development of fast inactivation was significantly faster with the mutant over the whole range of potentials and the largest difference was observed at −65mV, where $hNa_v1.1$-Q1478K showed a 2.3-fold faster kinetics than the wild-type (Fig. 2C). Thus, the shift of the inactivation curve is a real modification of the voltage

dependence of the channel, because it cannot be caused by the acceleration of the rate of development of fast inactivation of $hNa_v1.1$-Q1478K. These modifications are consistent with opposite effects on neuronal excitability: the positive shift of the inactivation curve is consistent with neuronal hyperexcitability, because at the typical resting potential of −65mV about 50% of $hNa_v1.1$-Q1478K current is inactivated, compared with about 65% of wild type current; the acceleration of the development of inactivation is consistent with hypoexcitability because $hNa_v1.1$-Q1478K current can be inactivated by shorter depolarizations.

Since we observed modifications of the kinetics of development of fast inactivation, we investigated whether also other kinetic properties were modified. We studied the kinetics of the recovery from fast inactivation applying a 100ms-long inactivating pulse to 0mV followed by recovery interpulses of increasing duration to potentials between −115 and −95mV and by a test pulse to −5mV. The recovery curves were well fit by a single exponential relationship, as shown by the mean curves obtained with an interpulse potential of −95mV, displayed in Fig. 2D. The recovery at −95mV was about 2-fold faster with $hNa_v1.1$-Q1478K and significantly faster over the whole range of potentials tested (Fig. 2E). This effect is consistent with increased neuronal excitability, because $hNa_v1.1$-Q1478K current can recover more rapidly after short depolarizations.

Thus, Q1478K modifies the voltage dependence of inactivation and the kinetics of development of fast inactivation and of recovery from fast inactivation. These properties depend on the transitions among the closed and the closed-inactivated states of the channel (they are studied at potentials at which the channel is closed). Therefore, Q1478K can modify the properties of the inactivation from the closed states but not those of the inactivation from the open state, because the decay of the current was not modified (see above).

Slow inactivation

Long depolarizations induce in Na^+ channels a process of slow inactivation that is kinetically and mechanistically distinct from fast inactivation (Goldin, 2003). The properties of the slow inactivation may be particularly important for the pathogenesis of migraine, because neurons undergo long lasting depolarizations during CSD. We initially used a 1s-long inactivating pulse to −5mV in order to study the properties of both slow and fast inactivation. Recovery at −95mV after this pulse clearly showed two phases well described by a double exponential relationship, corresponding to recovery from fast and slow inactivation (Fig. 3A). Notably, the slow phase of recovery was about 81% of total recovery for $hNa_v1.1$-Q1478K, but only 43% for the wild type channel. This is consistent with a faster entry of $hNa_v1.1$-Q1478K into a slow inactivated state during the 1s long inactivating pulse, and shows that after relatively long depolarizations the mutant channel can generate less current than the wild type, consistently with neuronal hypoexcitability. The fast phase of recovery was about 3-fold faster for Q1478K, consistently with the data obtained studying the recovery from fast inactivation, and slow recovery was not significantly different with this protocol of stimulation. However, the value of the time constants derived from these data may not be accurate because of the commixture between recovery from fast and slow inactivation.

To more accurately characterize the properties of slow inactivation, we used other stimulation protocols. We studied the development of slow inactivation using inactivating prepulses to −5mV of increasing duration, followed by 15ms repolarizations to −95mV to allow complete recovery from fast inactivation. The curves were well fit by a single exponential relationship and reached the steady-state after about 20s (Fig. 3B). As inferred from the analysis of recovery from a 1s-long inactivating prepulse (see above), $hNa_v1.1$-Q1478K showed indeed a 2.1-fold faster entry into the slow inactivated state than wild type. The voltage dependence of the development of slow inactivation was studied with 20s-long prepulses at various potentials followed by 15ms repolarizations to −95mV, and was not modified by the mutation (Fig 3C). We studied the recovery from slow inactivation applying 20s-long inactivating prepulses to −5mV followed by recovery interpulses at −95mV of increasing duration (Fig. 3D). The recovery curve was well fit by the sum of two exponentials and was faster for $hNa_v1.1$-Q1478K: the faster time constant of recovery of the wild type was about 2.2-fold larger than that of $hNa_v1.1$-Q1478K, whereas the slower time constant did not show significant modifications. Thus, these experiments disclosed the acceleration of the faster phase of recovery from slow inactivation caused by Q1478K, which is consistent with neuronal hyperexcitability because $hNa_v1.1$-Q1478K current can recover more rapidly from long depolarizations. The voltage dependence of the recovery was studied applying a 20s inactivating prepulse to −5mV followed by a 20s recovery interpulse at various potentials, and was not significantly modified by the mutation (Fig. 3E).

Our results indicate that, in contrast with the findings obtained with $Na_v1.5$ (Dichgans et al., 2005), Q1478K has several effects on $hNa_v1.1$ properties. We observed a reduction of the current density, a positive shift of the voltage dependence of inactivation, a larger I_{NaP}, and a faster development of recovery from fast and slow inactivation. These results are intriguing because some of the modifications are consistent with neuronal hyperexcitability and others with hypoexcitability. Therefore, we furthered our study by applying stimuli that can disclose the overall effect of the mutation.

Overall effect of Q1478K in tsA-201 cells: use dependence of wild type and mutant channels

We simulated neuronal firing by applying trains of 2ms-long depolarizing steps to −5mV at different frequencies. Fig. 4A shows normalized currents elicited by steps applied from a holding potential of −105mV. At lower stimulation frequency (10Hz and 50Hz) the

mutant channel showed similar or more pronounced use dependence than the wild type. At higher stimulation frequency (100Hz and 200Hz) the current elicited with $hNa_v1.1$-Q1478K was larger in the initial part of the train, but the decay during the stimulation was more pronounced. Thus, at the end of the train $hNa_v1.1$- Q1478K current was smaller than the wild type current. Fig. 4B shows the results obtained applying the trains of stimulation from a more physiological holding potential of −70mV. At lower frequency (10Hz) the use dependence of $hNa_v1.1$-Q1478K was similar to that of the wild type. At higher frequency (50, 100 and 200Hz) the mutant had larger current at the beginning of the train in comparison with the wild type (this difference was larger than in the experiments done with holding potential of −105mV, see Fig. 4A), but in the final part of the train the curves converged and thus the two channels elicited similar current at the end of the 200-pulse train.

These results suggest that $hNa_v1.1$-Q1478K can sustain high frequency firing better than $hNa_v1.1$. However, during prolonged high frequency discharges the mutant becomes less effective than the wild type or comparable to it, probably because during these discharges the loss of function caused by the faster development of inactivation of the mutant counteracts the gain of function caused by other modifications. Interestingly, these modifications have not been described for Na^+ channel epileptogenic mutations, thus they may be typical of migraine mutations.

Functional study in transfected neurons

Na^+ channel properties are sensitive to the cell background (Baroudi et al., 2000;Chen et al., 2000;Cummins et al., 2001;Mantegazza et al., 2005b), thus we tested if the effects that we have observed in tsA-201 cells were conserved in a neuronal cell background. We transfected neocortical neurons in short-term primary cultures (30 hours after plating) obtained from P1-P3 rats. The neocortex is a brain structure involved in the generation of migraine, thus appropriate for studying the effects of FHM mutations. Moreover, we have previously showed that these cultured neurons have relatively small endogenous Na^+ current, making possible the selective study of exogenous transfected Na^+ channel subunits, which are expressed at much higher levels than the endogenous ones (Scalmani et al., 2006). However, cultured neurons develop processes that do not allow, using the whole-cell configuration of the patch-clamp technique, adequate voltage and space clamp control of the neuronal membrane required for the analysis of the gating of Na^+ channels. Thus, we used the on-cell macropatch configuration to record macroscopic Na^+ currents from a relatively large patch of membrane under good voltage and space clamp conditions, as in (Scalmani et al., 2006).

Fig. 5A shows average macropatch traces recorded applying a depolarizing step to −15mV. The mutation did not have any significant effects on the kinetics of activation or inactivation (Fig. 5A, inset). The Na^+ current begun to activate around −5mV and peaked at −5mV in both the conditions, as displayed by the I-V plot in Fig. 5B. We observed a 36% reduction in peak current in neurons transfected with Q1478K (Fig. 5C), which is similar to the reduction observed in tsA-201 cells. The voltage dependence of activation was not modified (Fig. 5D), but the voltage dependence of inactivation, studied applying 100ms-long inactivating prepulses at the indicated potentials, showed a 5mV positive shift (Fig. 5E), consistently with the results obtained in tsA-201 cells. Notably, I_{NaP} was virtually absent in the whole range of potentials both with $hNa_v1.1$ and $hNa_v1.1$-Q1478K (Fig. 5A). I_{NaP} may have been too small to be resolved in some recordings, where I_{NaT} was particularly small (smallest peak currents were 64pA for $hNa_v1.1$-Q1478K and 95pA for $hNa_v1.1$); however, in some recordings I_{NaT} was large enough for good resolution of I_{NaP} (maximum peak currents were 226pA for $hNa_v1.1$-Q1478K and 263pA for $hNa_v1.1$). Thus, in transfected neurons Q1478K did not induce an increase of I_{NaP}.

It is extremely challenging to study with classical stimulation protocols the properties of slow inactivation in transfected cultured neurons, because recordings can last in general just some minutes, a duration that is not sufficient for the application of the long slow inactivation stimulation protocols. Thus, in order to disclose the overall effect of the mutation, we applied as voltage stimulus a physiological neuronal discharge recorded in neocortical slices from a regular spiking adapting pyramidal neuron, as in (Mantegazza et al., 1998). This stimulus reproduces the physiological dynamic conditions of a firing neuron and can disclose the modifications of both the fast and the slow gating properties of Na^+ channels. The discharge was characterized by an initial frequency of 208 Hz gradually decreasing to 37 Hz (Fig. 6A). Fig. 6B displays mean macropatch Na^+ currents recorded in pyramidal neurons transfected with wild type or mutant channels, normalized for each patch to the maximum I_{NaT} derived from the I-V plot of the patch. The current elicited with the mutant channel was larger than with the wild type, as it is shown in the insets. To have a measurement representative of the whole time curse of the current elicited by an action potential (action current), we integrated the action currents and compared their areas. Fig. 6C shows the comparison of the areas subtended by normalized wild type and mutant action currents. Most of $hNa_v1.1$-Q1478K areas resulted significantly larger, consistently with a potentiation of the firing of the neurons that express $hNa_v1.1$-Q1478K.

To investigate the effect of long lasting depolarizations, we applied the discharge preceded by a 1s depolarizing prepulse to −5mV. Using this stimulation, the action currents were quite small both with $hNa_v1.1$-Q1478K and wild type channel. However, wild type currents were significantly larger for the first action potential of the discharge and for some action potentials later on, as shown by the comparison of the areas of the action currents displayed in Fig. 6D. This results is consistent with an enhanced inhibition of $hNa_v1.1$-Q1478K and a reduced ability to sustain neuronal firing after long depolarizations.

Therefore, the results obtained in neurons are similar to those obtained in tsA-201 cells, even if in neurons the effects that we have observed are smaller.

Discussion

The $Na_v1.1$ FHM mutations Q1478K (Q1489K in the longer isoform) and L1638Q (L1649Q) have been previously studied using $Na_v1.5$ Na^+ channel. Q1478K caused an accelerated recovery from fast inactivation of $Na_v1.5$ (Dichgans et al., 2005). L1649Q, which is located in the trasmembrane segment S4 of DIV (a voltage-sensor that is particularly important for fast inactivation), caused an acceleration of the recovery from fast inactivation and a decrease of the rate of fast inactivation (current decay) of $Na_v1.5$ (Vanmolkot et al., 2007). These effects induce a gain of function and are consistent with increased neuronal excitability and accumulation of extracellular K^+ and glutamate, thus they may facilitate CSD. However, the effects are similar to those of some epileptogenic mutations of $Na_v1.1$.

Our results show that the effects of Q1478K in $hNa_v1.1$ are different than in $hNa_v1.5$ and can account for the different pathogenic mechanism of migraine mutations in comparison with epileptogenic mutations. We observed modifications of several of the properties of fast and slow inactivation, both in tsA-201 cells and in transfected neurons. In tsA-201 the rate of recovery from inactivation was accelerated similarly to $hNa_v1.5$, but we observed also an increase in the rate of development of fast inactivation and a positive shift of its voltage dependence, thus a modification of the properties of the transitions occurring among the closed and the inactivated states of the channel. The rate of decay of the current (the transition from the open state to the open-inactivated state) was not modified, but I_{NaP} was significantly increased. The rate of development of slow inactivation and of recovery from slow inactivation was also accelerated. Moreover, current density was significantly reduced, but activation properties were not modified.

In transfected neurons we studied the properties of $hNa_v1.1$-Q1478K using as voltage stimuli both classical voltage steps and trains of action potentials. We recorded Na^+ currents with the on-cell patch-clamp configuration, thus with no rupture of the plasma membrane and no dialysis of the cytoplasm. The effects were similar to those observed using tsA-201 cells, but less pronounced. Notably, I_{NaP} was virtually absent in transfected neurons both with wild type and $hNa_v1.1$-Q1478K channels, consistently with the decrease in I_{NaP} amplitude that we observed during long lasting recordings in tsA-201 cells transfected with $hNa_v1.1$-Q1478K. Interestingly, I_{NaP} can be potentiated by a G-protein mediated modulation (Mantegazza et al., 2005b) and in our whole-cell recordings from tsA-201 cells we used a fluoride-based intracellular solution that can interfere with the modulation. Consistently, I_{NaP} amplitude of wild type currents in this study was much lower in comparison with that obtained using a different intracellular recording solution, as in (Mantegazza et al., 2005b). Thus, the initial difference in INa_p amplitude that we observed may be due to a Q1478K-dependent sensitization of the mutant to a modulation, rather than to the modification of an intrinsic property of the α subunit. Na^+ channels may be in a non-modulated state in neonatal neurons in culture, consistently with data that show an increase of I_{NaP} during postnatal development in cortical pyramidal neurons (Huguenard et al., 1988). In general, in neurons I_{NaP} is very small in comparison with tsA-201 cells and probably its increase is tightly controlled because even small enhancements would cause major modifications of neuronal function.

Consistently with its position within the inactivation loop (DIII-IV linker) (Catterall, 2000), Q1478K affected several properties of fast inactivation but did not alter activation properties. Interestingly, the mutation modified also the kinetic properties of slow inactivation, even if experimental evidences have shown that slow inactivation does not directly depend on DIII-IV linker (Goldin, 2003). Thus, this points to a role of amino acids in DIII-IV linker in setting the properties of slow inactivation.

Interestingly, some of the effects that we have observed cause a loss of function of the channel, others a gain of function. Thus, some of them are consistent with cellular hyperexcitability, others with hypoexcitability. We showed that the overall effect is an initial enhanced capacity to sustain high frequency neuronal discharges, and, notably, that this capacity is retained for a limited period during long lasting discharges, evidently because the modifications that are consistent with a loss of function become dominant during the discharge. Thus, Q1478K can cause a pronounced but self-limited neuronal hyperexcitability, and in some conditions can lead to hypoexcitability. In fact, during some long lasting trains of stimulation (which reproduce excessive neuronal firing) the elicited current became smaller than the wild type current, and Q1478K generated less current than the wild type channel also after long lasting depolarizations, a key event in the pathogenesis of migraine.

The reduction in peak current amplitude is a loss of function effect that we excluded from the analysis of the overall effect (Fig. 4 and Fig. 6), because the analysis was done with normalized traces. However, GABAergic interneurons are particularly sensitive to the loss of $Na_v1.1$ in knock-out mice, even if $Na_v1.1$ is expressed both in GABAergic interneurons and in glutamatergic pyramidal neurons (Yu et al., 2006); thus, the reduction caused by Q1478K may also be more pronounced in interneurons, causing network hyperexcitability. Moreover, an increase in I_{NaP} can have larger effects on neuronal firing than a moderate decrease in peak current amplitude (Mantegazza et al., 1998).

$Na_v1.1$ is the major target of epileptogenic mutations (Meisler and Kearney, 2005;Avanzini et al., 2007), but, interestingly, just few cases of seizures have been reported in FHM patients (Dichgans et al., 2005;Vanmolkot et al., 2007). Thus, FHM mutations should modify

$Na_v1.1$ function differently than epileptogenic mutations. Fig. 7 illustrates the effects of Q1478K in the context of the current scheme of pathogenic mechanism of migraine (Pietrobon and Striessnig, 2003). In migraine the genetic background is important in determining an intrinsic migraine threshold that is modulated by internal and external factors (trigger stimuli); emotional stress and minor head trauma are among the most common triggers of FHM attacks (Dichgans et al., 2005;Pietrobon, 2007). Migraine triggers are thought to induce excessive neuronal firing and consequently lead to extracellular K^+ and glutamate accumulation, eventually leading to enhanced long-lasting neuronal depolarization and silencing of firing caused by inactivation of Na^+ channels, thus producing CSD, which causes aura and, through still unclear mechanisms, activation of trigeminal pain afferents and headache (Pietrobon and Striessnig, 2003;Pietrobon, 2007).

Some of the effects of Q1478K can facilitate the development of FHM attacks: the positive shift of the inactivation curve, the acceleration of the recovery from fast and slow inactivation, and the increase of I_{NaP} may lead to excessive neuronal firing subsequently to a trigger stimulus, thus to accumulation of extracellular K+ and glutamate. Decreased peak current amplitude could reduce excessive firing, but it might be interneuron specific (see above) and thus potentiate hyperexcitability. The increase of I_{NaP} might also be cell type specific because it may be due to an enhanced modulation of the mutant channel. In general, excessive firing may be cell type specific, but also a non-specific increase in neuronal excitability would lead to accumulation of extracellular K^+. Subsequently to the induction of hyperexcitability, the acceleration of the development of slow inactivation may facilitate the silencing of firing and the development of CSD.

Importantly, some of the effects that we have observed can counteract neuronal hyperexcitability: the acceleration of the development of fast and slow inactivation can limit excessive firing during prolonged discharges, as we have shown applying trains of high frequency stimulations, and thus effectively counteract the development of epileptic seizures. The acceleration of the recovery from slow inactivation can counteract the silencing of firing, but it should be more effective during the repolarization after a long depolarization, and thus in the recovery from CSD and not in the development of the migraine attack.

Epileptogenic mutations of $Na_v1.1$ cause variable functional defects (Meisler and Kearney, 2005;Avanzini et al., 2007), but the functional defects that we have observed for Q1478K are different than those described thus far for epileptogenic mutants. In particular, the potent but self-limited capacity to induce neuronal hyperexcitability that in some conditions can invert to induction of hypoexcitability (see Fig. 4) may be a specific characteristic of $Na_v1.1$ migraine mutations, able to both trigger the cascade of events that leads to migraine and block the development of extreme hyperexcitability that generate epileptic seizures.

Thus, we have disclosed at the channel biophysical level a possible difference in the pathogenic mechanism of two major neurological diseases caused by $Na_v1.1$ mutations.

Ackowledgements:

We thank Dr. Jeff Clare and Dr. Al George for sharing DNA clones, and Dr. Giuliano Avanzini for support. The study was supported by the European Integrated Project “EPICURE” (EFP6–037315) to MM and SF and by a fellowship from the Italian League Against Epilepsy to RR.

Abbreviations

CSD: cortical spreading depression

FHM: familial hemiplegic migraine

I_{NaT} : “transient” rapidly inactivating component of the Na^+ current

I_{NaP} : “persistent” slowly inactivating component of the Na^+ current

References:

Reference List

- Avanzini G , Franceschetti S , Mantegazza M 2007; Epileptogenic channelopathies: experimental models of human pathologies. Epilepsia. 48: (Suppl 2) 51- 64
- Baroudi G , Carbonneau E , Pouliot V , Chahine M 2000; SCN5A mutation (T1620M) causing Brugada syndrome exhibits different phenotypes when expressed in Xenopus oocytes and mammalian cells. FEBS Lett. 467: 12- 16
- Bolay H , Reuter U , Dunn AK , Huang Z , Boas DA , Moskowitz MA 2002; Intrinsic brain activity triggers trigeminal meningeal afferents in a migraine model. Nat Med. 8: 136- 142
- Bowyer SM , Aurora KS , Moran JE , Tepley N , Welch KM 2001; Magnetoencephalographic fields from patients with spontaneous and induced migraine aura. Ann Neurol. 50: 582- 587
- Catterall WA 2000; From ionic currents to molecular mechanisms: the structure and function of voltage-gated sodium channels. Neuron. 26: 13- 25
- Catterall WA , Goldin AL , Waxman SG 2005; International Union of Pharmacology. XLVII. Nomenclature and structure-function relationships of voltage-gated sodium channels. Pharmacol Rev. 57: 397- 409
- Chen YH , Dale TJ , Romanos MA , Whitaker WR , Xie XM , Clare JJ 2000; Cloning, distribution and functional analysis of the type III sodium channel from human brain. Eur J Neurosci. 12: 4281- 4289
- Cummins TR , Aglieco F , Renganathan M , Herzog RI , Dib-Hajj SD , Waxman SG 2001; Nav1.3 sodium channels: rapid repriming and slow closed-state inactivation display quantitative differences after expression in a mammalian cell line and in spinal sensory neurons. J Neurosci. 21: 5952- 5961
- De Fusco M , Marconi R , Silvestri L , Atorino L , Rampoldi L , Morgante L , Ballabio A , Aridon P , Casari G 2003; Haploinsufficiency of ATP1A2 encoding the Na+/K+ pump alpha2 subunit associated with familial hemiplegic migraine type 2. Nat Genet. 33: 192- 196

- Dichgans M , Freilinger T , Eckstein G , Babini E , Lorenz-Depiereux B , Biskup S , Ferrari MD , Herzog J , van den Maagdenberg AM , Pusch M , Strom TM 2005; Mutation in the neuronal voltage-gated sodium channel SCN1A in familial hemiplegic migraine. Lancet. 366: 371- 377
- Goldin AL 2003; Mechanisms of sodium channel inactivation. Curr Opin Neurobiol. 13: 284- 290
- Hadjikhani N , Sanchez DR , Wu O , Schwartz D , Bakker D , Fischl B , Kwong KK , Cutrer FM , Rosen BR , Tootell RB , Sorensen AG , Moskowitz MA 2001; Mechanisms of migraine aura revealed by functional MRI in human visual cortex. Proc Natl Acad Sci U S A. 98: 4687- 4692
- Huguenard JR , Hamill OP , Prince DA 1988; Developmental changes in Na+ conductances in rat neocortical neurons: appearance of a slowly inactivating component. J Neurophysiol. 59: 778- 795
- Kirsch GE , Brown AM 1989; Kinetic properties of single sodium channels in rat heart and rat brain. J Gen Physiol. 93: 85- 99
- Kors EE , Vanmolkot KR , Haan J , Frants RR , van den Maagdenberg AM , Ferrari MD 2004; Recent findings in headache genetics. Curr Opin Neurol. 17: 283- 288
- Mantegazza M , Cestele S 2005; Beta-scorpion toxin effects suggest electrostatic interactions in domain II of voltage-dependent sodium channels. J Physiol. 568: 13- 30
- Mantegazza M , Franceschetti S , Avanzini G 1998; Anemone toxin (ATX II)-induced increase in persistent sodium current: effects on the firing properties of rat neocortical pyramidal neurones. J Physiol. 507 : (Pt 1) 105- 116
- Mantegazza M , Gambardella A , Rusconi R , Schiavon E , Annesi F , Cassulini RR , Labate A , Carrideo S , Chifari R , Canevini MP , Canger R , Franceschetti S , Annesi G , Wanke E , Quattrone A 2005a; Identification of an Nav1.1 sodium channel (SCN1A) loss-of-function mutation associated with familial simple febrile seizures. Proc Natl Acad Sci U S A. 102: 18177- 18182
- Mantegazza M , Yu FH , Catterall WA , Scheuer T 2001; Role of the C-terminal domain in inactivation of brain and cardiac sodium channels. Proc Natl Acad Sci U S A. 98: 15348- 15353
- Mantegazza M , Yu FH , Powell AJ , Clare JJ , Catterall WA , Scheuer T 2005b; Molecular determinants for modulation of persistent sodium current by G-protein betagamma subunits. J Neurosci. 25: 3341- 3349
- Meisler MH , Kearney JA 2005; Sodium channel mutations in epilepsy and other neurological disorders. J Clin Invest. 115: 2010- 2017
- Noda M , Ikeda T , Kayano T , Suzuki H , Takeshima H , Kurasaki M , Takahashi H , Numa S 1986; Existence of distinct sodium channel messenger RNAs in rat brain. Nature. 320: 188- 192
- Oliveira JS , Redaelli E , Zaharenko AJ , Cassulini RR , Konno K , Pimenta DC , Freitas JC , Clare JJ , Wanke E 2004; Binding specificity of sea anemone toxins to Nav 1.1–1.6 sodium channels: unexpected contributions from differences in the IV/S3-S4 outer loop. J Biol Chem. 279: 33323- 33335
- Ophoff RA , Terwindt GM , Vergouwe MN , van Eijk R , Oefner PJ , Hoffman SM , Lamerdin JE , Mohrenweiser HW , Bulman DE , Ferrari M , Haan J , Lindhout D , van Ommen GJ , Hofker MH , Ferrari MD , Frants RR 1996; Familial hemiplegic migraine and episodic ataxia type-2 are caused by mutations in the Ca2+ channel gene CACNL1A4. Cell. 87: 543- 552
- Pietrobon D 2007; Familial hemiplegic migraine. Neurotherapeutics. 4: 274- 284
- Pietrobon D , Striessnig J 2003; Neurobiology of migraine. Nat Rev Neurosci. 4: 386- 398
- Richmond JE , Featherstone DE , Hartmann HA , Ruben PC 1998; Slow inactivation in human cardiac sodium channels. Biophys J. 74: 2945- 2952
- Rusconi R , Scalmani P , Cassulini RR , Giunti G , Gambardella A , Franceschetti S , Annesi G , Wanke E , Mantegazza M 2007; Modulatory proteins can rescue a trafficking defective epileptogenic Nav1.1 Na+ channel mutant. J Neurosci. 27: 11037- 11046
- Scalmani P , Rusconi R , Armatura E , Zara F , Avanzini G , Franceschetti S , Mantegazza M 2006; Effects in neocortical neurons of mutations of the Na(v)1.2 Na+ channel causing benign familial neonatal-infantile seizures. J Neurosci. 26: 10100- 10109
- Schaller KL , Krzemien DM , McKenna NM , Caldwell JH 1992; Alternatively spliced sodium channel transcripts in brain and muscle. J Neurosci. 12: 1370- 1381
- Silberstein SD 2004; Migraine. Lancet. 363: 381- 391
- van den Maagdenberg AM , Pietrobon D , Pizzorusso T , Kaja S , Broos LA , Cesetti T , van de Ven RC , Tottene A , van der KJ , Plomp JJ , Frants RR , Ferrari MD 2004; A Cacna1a knockin migraine mouse model with increased susceptibility to cortical spreading depression. Neuron. 41: 701- 710
- Vanmolkot KR , Babini E , de Vries B , Stam AH , Freilinger T , Terwindt GM , Norris L , Haan J , Frants RR , Ramadan NM , Ferrari MD , Pusch M , van den Maagdenberg AM , Dichgans M 2007; The novel p.L1649Q mutation in the SCN1A epilepsy gene is associated with familial hemiplegic migraine: genetic and functional studies. Mutation in brief #957. Online. Hum Mutat. 28: 522-
- Yu FH , Mantegazza M , Westenbroek RE , Robbins CA , Kalume F , Burton KA , Spain WJ , McKnight GS , Scheuer T , Catterall WA 2006; Reduced sodium current in GABAergic interneurons in a mouse model of severe myoclonic epilepsy in infancy. Nat Neurosci. 9: 1142- 1149

Figure 1

Effects of Q1478K on activation properties and persistent current (I_{NaP}) in tsA-201 cells

A, representative whole-cell Na^+ currents (top $hNa_v1.1$, bottom $hNa_v1.1$-Q1478K) recorded with 75ms long depolarizing steps from −65mV to +55mV in 10mV increments, from a holding potential of −100mV (scale bars 500pA, 2.5ms); the insets show the first 4ms of the traces. B, average normalized currents ($hNa_v1.1$ solid line, $hNa_v1.1$-Q1478K dashed line) elicited with a depolarizing step to −15mV, the error bars are the standard error of the mean of selected data points (scale bar 1ms); the inset shows the final 5ms of the 150ms long traces, to compare I_{NaP}. C, current density-voltage plots for $hNa_v1.1$ (black symbols, 174±14pA/pF, n=21) and $hNa_v1.1$-Q1478K (white symbols, 124±8pA/pF, n=45, p=0.009). D, mean voltage dependence of activation, the lines are Boltzmann relationships whose parameters were calculated averaging the parameters of the fits of the single cells: solid line $hNa_v1.1$ (Va=−34.2±0.9mV, Ka=8.2±0.4mV), dashed line $hNa_v1.1$-Q1478K (Va=−36.6±0.7mV, Ka=8.8±0.3mV). E, mean current-voltage plots for I_{NaP} recorded after 5min from the establishment of the whole-cell configuration: $hNa_v1.1$ 1.3±0.2%, $hNa_v1.1$-Q1478K 5.3±1.0% (p=0.002). F, mean current-voltage plots for I_{NaP} recorded after more than 17min: $hNa_v1.1$ 0.9±0.3% (20–60min, n=7), $hNa_v1.1$-Q1478K 1.2±0.2% (17–30min, n=6); the lines with no symbols are the I_{NaP} recorded in the same cells after 5min: $hNa_v1.1$ 1.2±0.2%, $hNa_v1.1$-Q1478K 4.5±0.6%.

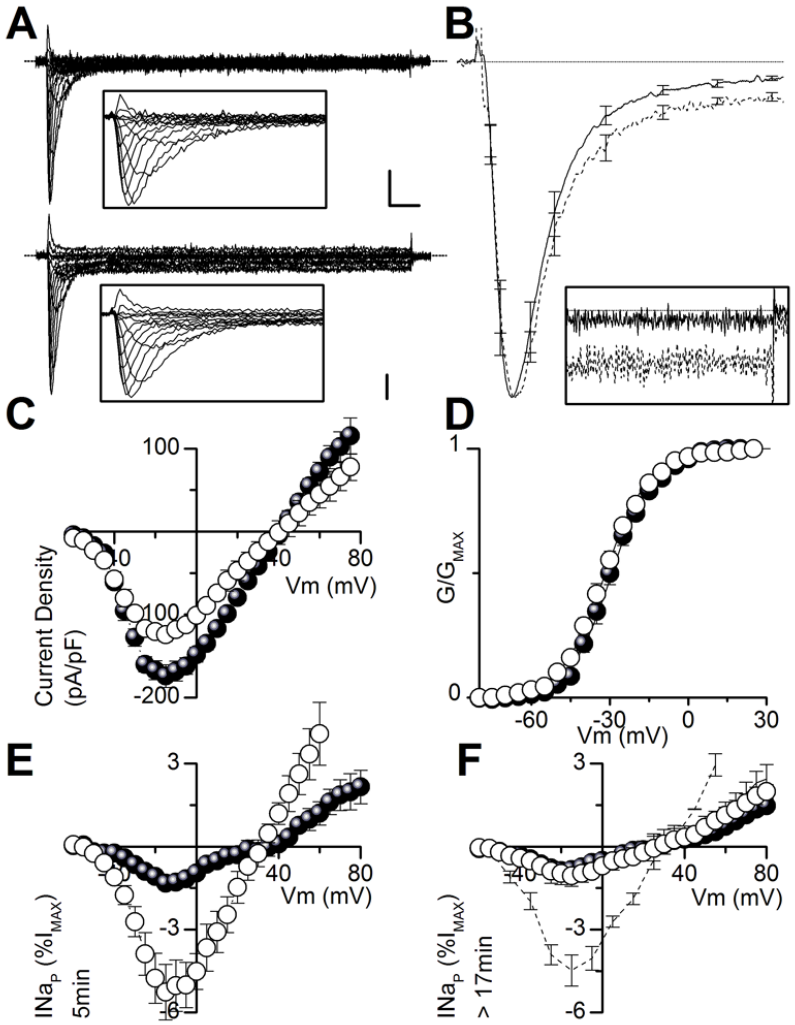

Figure 2

Effects of Q1478K on fast inactivation properties in tsA-201 cells

A, mean voltage dependence of fast inactivation (black symbols, $hNa_v1.1$; white symbols, $hNa_v1.1$-Q1478K); the lines are Boltzmann relationships with the following mean parameters: $hNa_v1.1$ (n=20) Vh=−69.3±0.5mV, Kh=7.3±0.4mV, baseline 0.017±0.008; $hNa_v1.1$-Q1478K (n=42), Vh=−65.2±0.5mV (p=0.006), Kh=7.4±0.3mV, baseline 0.057±0.07 (p=0.01). B, mean kinetics of development of fast inactivation at −65mV, the lines are mean fits of single exponential relationships. C, time constants of development over a range of potentials: −45mV, $hNa_v1.1$ (n=9) τ_{DEV}=3.9±0.6ms, $hNa_v1.1$-Q1478K, (n=14) τ_{DEV}=2.6±0.2ms (p=0.03); −55mV, $hNa_v1.1$ (n=12) τ_{DEV}=14.9±2.9ms, $hNa_v1.1$-Q1478K (n=16) τ_{DEV}=8.4±0.9ms (p=0.02); −65mV, $hNa_v1.1$ (n=13) τ_{DEV}=40.6±5.5ms, $hNa_v1.1$-Q1478K (n=21) τ_{DEV}=17.6±1.9ms ($p=6*10^{-5}$); −75mV, $hNa_v1.1$ (n=9) τ_{DEV}=35.7±2.9ms, $hNa_v1.1$-Q1478K (n=9) τ_{DEV}=14.4±2.5ms ($p<10^{-5}$). D, mean kinetics of recovery at −95mV from a 100ms inactivating pulse to 0mV, the lines are mean fits of single exponential relationships to the data; E, time constants of recovery over a range of potentials: −95mV, $hNa_v1.1$ (n=11) τ_{REC}=6.6±0.4ms, $hNa_v1.1$-Q1478K (n=20) τ_{REC}=3.4±0.2ms ($p<10^{-5}$); −105mV, $hNa_v1.1$ (n=9) τ_{REC}=4.2±0.4ms, $hNa_v1.1$-Q1478K (n=17) τ_{REC}=2.2±0.1ms ($p<10^{-5}$); −115mV, $hNa_v1.1$ (n=8) τ_{REC}=3.0±0.1ms, $hNa_v1.1$-Q1478K (n=13) τ_{REC}=1.8±0.1ms ($p<10^{-5}$).

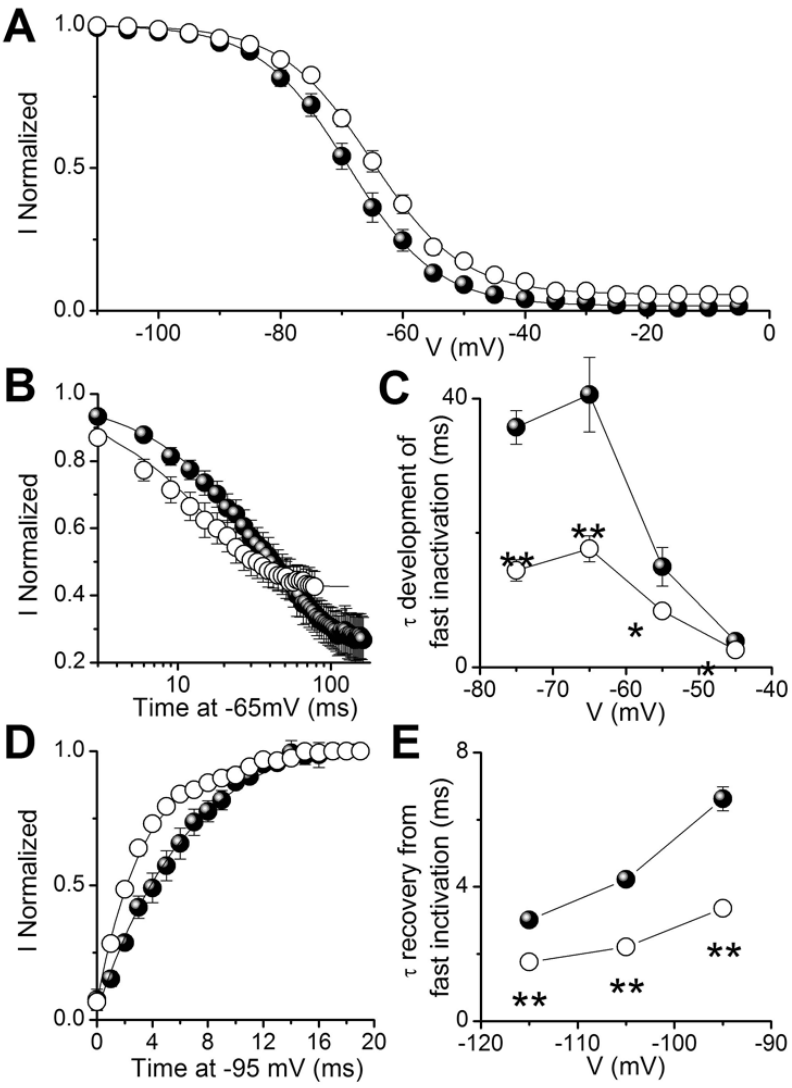

Figure 3

Effects of Q1478K on slow inactivation properties in tsA-201 cells

A, mean recovery at −95mV from a 1s inactivating pulse to −5mV (black symbols, $hNa_v1.1$; white symbols, $hNa_v1.1$-Q1478K), the lines are mean fits of double exponential relationships with the following parameters: $hNa_v1.1$ (n=9) τ_{FAST}=6.9±1ms A_1=0.59±0.06, τ_{SLOW}=976±110ms A_2=0.41±0.05; $hNa_v1.1$-Q1478K (n=10) τ_{FAST}=2.4±0.8ms (p=$5*10^{-5}$) A_1=0.22±0.05 (p<10^{-5}), τ_{SLOW}=1083±102ms A_2=0.78±0.06 (p<10^{-5}). B, mean development of slow inactivation at −5mV, the lines are mean fits of exponential relationships with the following parameters: $hNa_v1.1$ (n=6) τ_{DEV}=2090±240ms baseline=0.10±0.05; $hNa_v1.1$-Q1478K (n=7) τ_{DEV}=938±91ms (p=0.02) baseline=0.06±0.04. C, voltage dependence of development obtained with a 20s inactivating prepulse, the lines are Boltzmann relationships with the following mean parameters: $hNa_v1.1$ (n=5) Vh=−75.8±1.3mV Kh=6.2±0.5 baseline=0.06±0.04; $hNa_v1.1$-Q1478K (n=6) Vh=−77.2±1.1mV Kh=7.7±0.4 baseline=0.08±0.04. D, mean recovery of slow inactivation at −95mV, the lines are mean fits of exponential relationships with the following parameters: $hNa_v1.1$ (n=12), τ_{REC1}=1319±550ms A1=0.35±0.16 τ_{REC2}=6403±1550ms A2=0.65±0.17; $hNa_v1.1$- Q1478K (n=14), τ_{REC1}=617±208ms (p=0.03) A1=0.23±0.14 τ_{REC2}=5555±431ms A2=0.77±0.16. E, voltage dependence of recovery obtained with a 20s inactivating prepulse, the lines are Boltzmann relationships with the following mean parameters: $hNa_v1.1$ (n=5) Vh=−60.4±2.3mV Kh=8.1±0.8; $hNa_v1.1$-Q1478K (n=5) Vh=−65.8±4.3mV Kh=7.1±0.7.

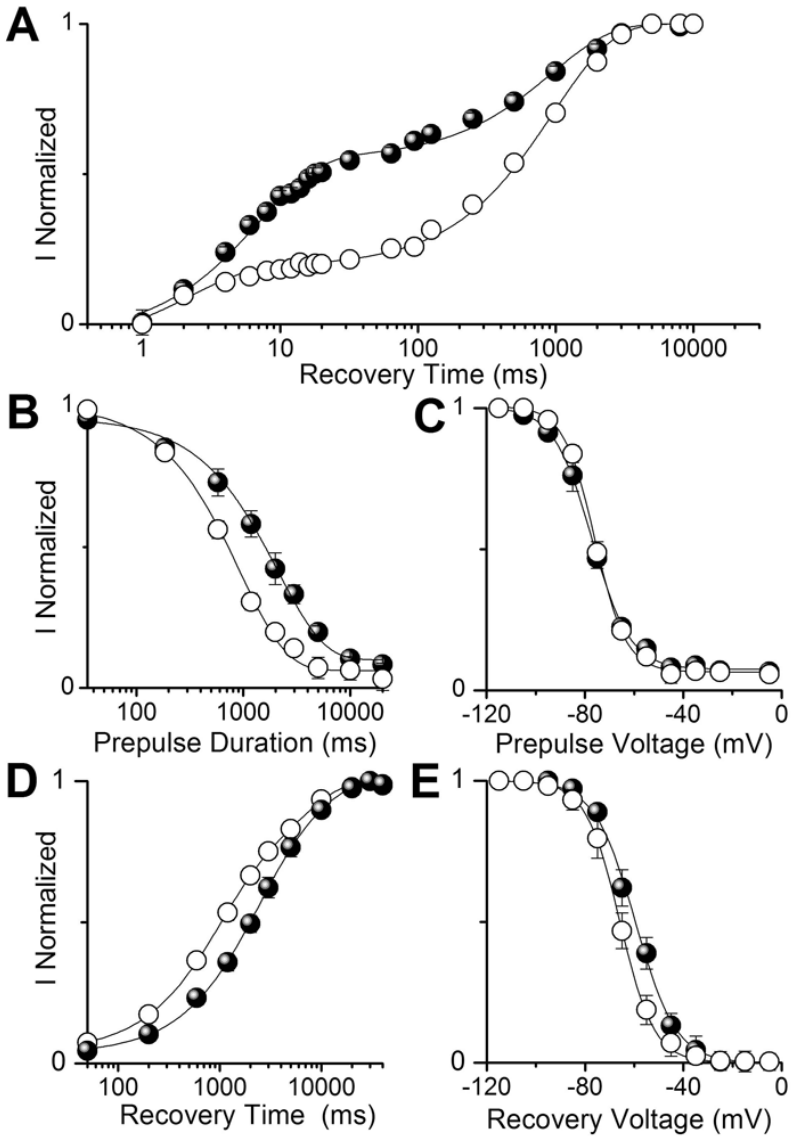

Figure 4

Overall effect of Q1478K studied with trains of depolarizing steps in tsA-201 cells

A, use dependence induced by trains of 200 depolarizing steps 2ms-long to −5mV from a holding potential of −105mV, at the frequencies indicated (black symbols, $hNa_v1.1$; white symbols, $hNa_v1.1$-Q1478K); the arrows indicate the intersections between the curves of wild type and mutant channels ($hNa_v1.1$: 10Hz n=16, 50Hz n=15, 100Hz n=19, 200Hz n=17; $hNa_v1.1$-Q1478K: 10Hz n=21, 50Hz n=19, 100Hz n=22, 200Hz n=19). B, similar stimuli as in A but applied from a holding potential of −70mV ($hNa_v1.1$: 10Hz n=14, 50Hz n=12, 100Hz n=13, 200Hz n=8; $hNa_v1.1$-Q1478K: 10Hz n=14, 50Hz n=13, 100Hz n=17, 200Hz n=8); the double arrows highlight the large difference between wild type and mutant channels at the beginning of the train.

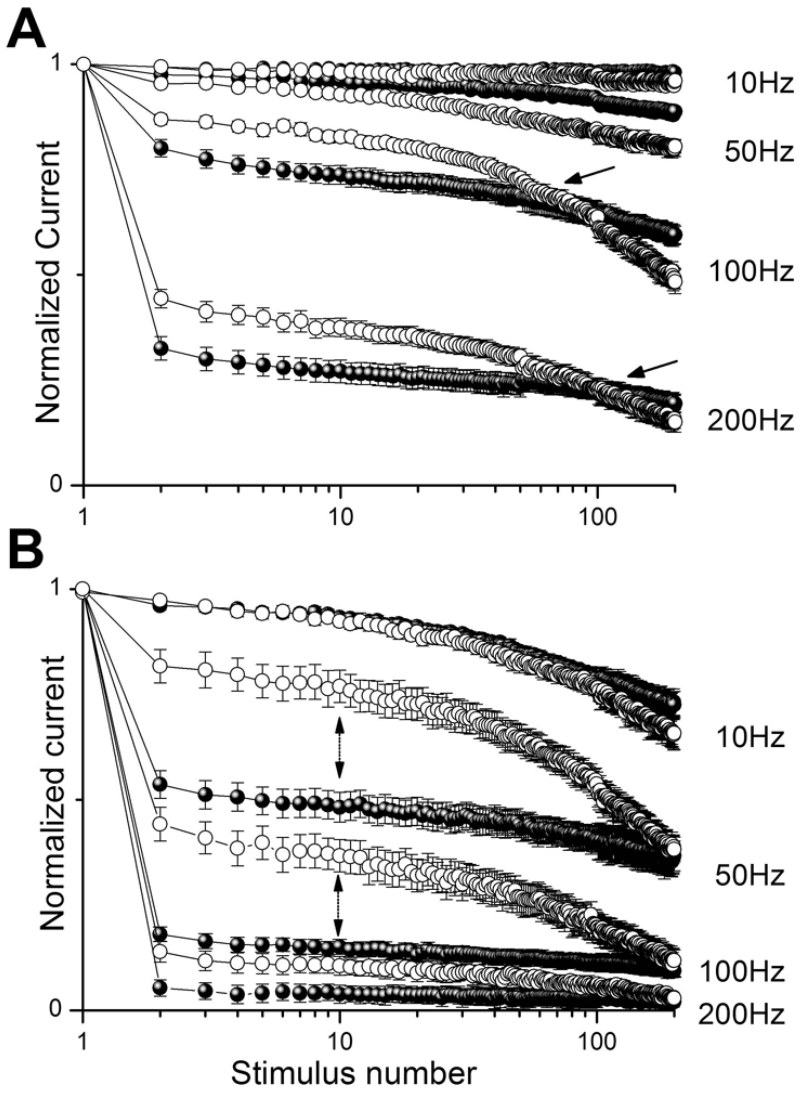

Figure 5
Effects of Q1478K in transfected neurons

A, average normalized macropatch currents elicited with a depolarizing step to −5mV from a holding potential of −95mV in neurons transfected with $hNa_v1.1$ (solid line) and $hNa_v1.1$-Q1478K (dashed line); calibration bar 5ms. The inset shows the first 3.2ms of the traces. B, Normalized current-voltage plots for $hNa_v1.1$ (black symbols, n=12) and $hNa_v1.1$-Q1478K (white symbols, n=14). C, bar-graph showing mean macropatch maximum current amplitudes: $hNa_v1.1$ 173±22pA, $hNa_v1.1$-Q1478K 112±14pA (p=0,008). D, mean voltage dependence of activation, the lines are Boltzmann relationships whose mean parameters are: $hNa_v1.1$, Va=−24.5±1.4mV, Ka=7.9±0.8mV; $hNa_v1.1$-Q1478K, Va=−24.8±1.0mV, Ka=9.1±0.6mV. E, mean voltage dependence of inactivation, the lines are Boltzmann relationships with the following mean parameters: $hNa_v1.1$ (n=9), Vh=−65.1±1.1mV, Kh=6.0±0.5mV; $hNa_v1.1$-Q1478K (n=12), Vh=−60.1±0.8mV (p=0.03), Kh=7.4±0.5mV (p=0.04).

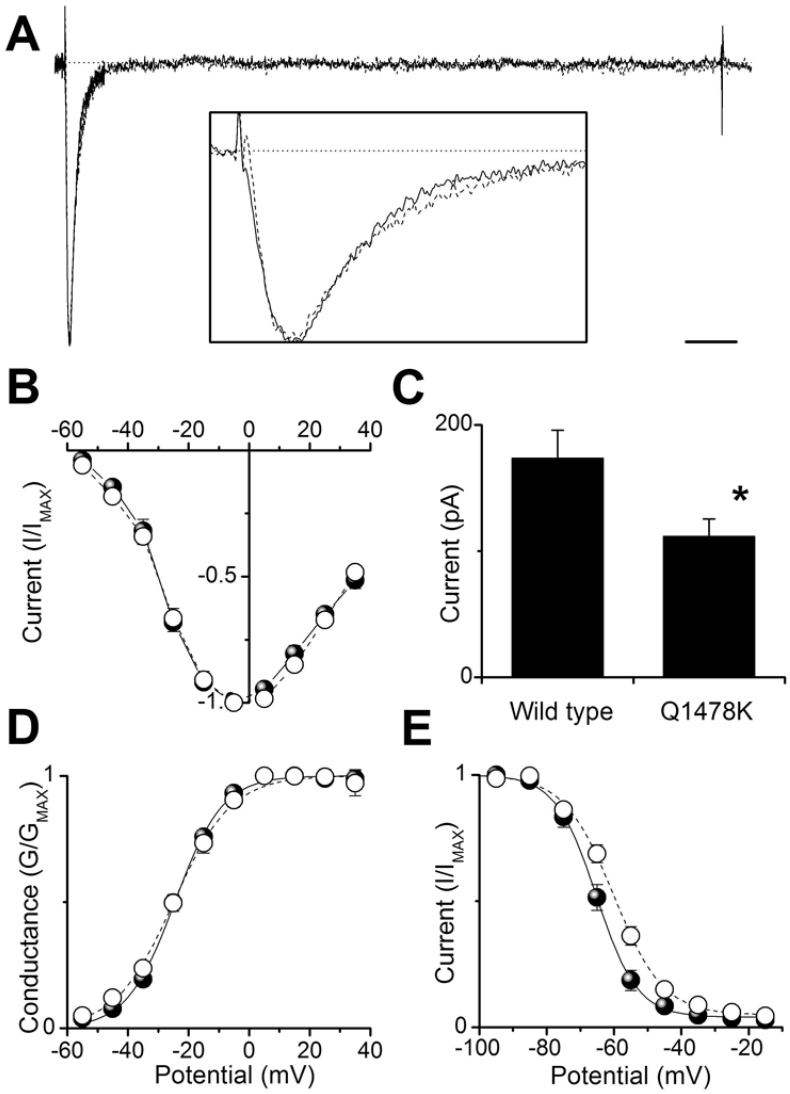

Figure 6

Overall effect of Q1478K studied with action potential clamp in transfected neurons

A, Action potential discharge recorded with sharp microelectrodes in a layer V neuron in neocortical slices injecting a 380ms depolarizing current step of 300pA. B, superimposed average macropatch currents elicited in neurons transfected with $hNa_v1.1$ (solid line, n=9) or $hNa_v1.1$-Q1478K (dashed line, n=13) applying as voltage stimulus the action potential discharge showed in A from a holding potential of −65mV; the insets show the enlargement of the underlined parts of the traces. C, average area subtended by each action current in the train for $hNa_v1.1$ (black symbols) and $hNa_v1.1$-Q1478K (white symbols). D, average area subtended by each action current when the train was preceded by a 1s inactivating prepulse to −5mV.

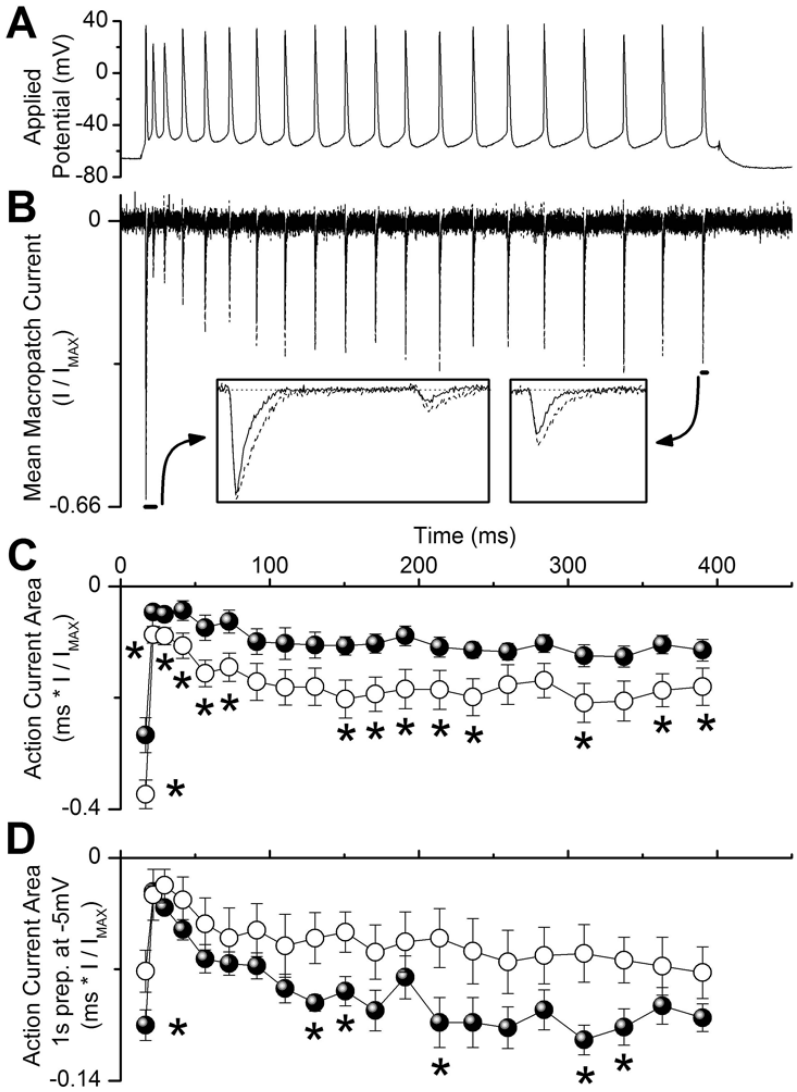

Figure 7

Effects of Q1478K in the context of the current scheme of pathogenic mechanism of migraine

Some of the modifications induced by Q1478K may facilitate the development of CSD, thus generating aura and ultimately triggering migraine. However, some of the modifications can limit these effects and may be able to counteract the generation of extreme hyperexcitability that would lead to seizures. For instance, acceleration of the development of fast and slow inactivation can limit the induction of excessive firing. Increase of I_{NaP} may be due to a modulation and decrease of I_{NaT} may be cell type specific. See text for details.